Applied Surface Science 367 (2016) 533–541

Contents lists available at ScienceDirect

Applied Surface Science

journal homepage: www.elsevier.com/locate/apsusc

Synthesis of mesoporous silica-coated magnetic nanoparticles modified with 4-amino-3-hydrazino-5-mercapto-1,2,4-triazole and its application as Cu(II) adsorbent from aqueous samples

Marcos Henrique P. Wondracek[a,e,*], Alexandre Oliveira Jorgetto[b,e], Adrielli Cristina P. Silva[b], Janaíne do Rocio Ivassechen[b,e], José Fabián Schneider[f], Margarida Juri Saeki[b], Valber Albuquerque Pedrosa[b], Walter Kenji Yoshito[c], Fabiano Colauto[d], Wilson A. Ortiz[d], Gustavo Rocha Castro[b]

[a] Faculdade de Ciências Exatas e Tecnologia – UFGD, C.P.533, 79804-970 Dourados, MS, Brazil
[b] Institute of Biosciences of Botucatu-UNESP – Chemistry and Biochemistry Department, C.P. 510, 18618-000 Botucatu, SP, Brazil
[c] Centro de Ciência e Tecnologia de Materiais – IPEN, 05508-000 São Paulo, SP, Brazil
[d] Departamento de Física-UFsCar, C.P. 676, 13565-905 São Carlos, SP, Brazil
[e] Institute of Chemistry-UNESP, 14800-060 Araraquara, SP, Brazil
[f] Department of Physics and Interdisciplinary Science, Institute of Physics of Sao Carlos – USP C.P. 369, 13560-970 Sao Carlos, SP, Brazil

ARTICLE INFO

Article history:
Received 13 August 2015
Received in revised form 14 January 2016
Accepted 19 January 2016
Available online 22 January 2016

Keywords:
Solid-phase extraction
Preconcentration
Aqueous samples
Adsorption models

ABSTRACT

This study presents an alternative, rapid, and environment-friendly synthesis procedure of a magnetic core–shell mesoporous SBA-15 silica composite, its functionalization with 4-amino-3-hydrazino-5-mercapto-1,2,4-triazole (Purpald), and its application in dispersive solid-phase microextraction (DSPME) for Cu(II) from water. The materials were characterized through magnetization measurements, scanning electron microscopy (SEM), high-resolution transmission electron microscopy (HR-TEM), Fourier transform infrared (FTIR), nuclear magnetic resonance (NMR) of ^{29}Si and ^{13}C, elemental analysis, and surface area measurements. FTIR and NMR analyses indicated the presence of the ligand on the functionalized material and that it was coupled through a C—S bond. TEM images clearly show that the magnetite core particles were effectively coated with a silica shell. The material presented a surface area of 287.99 $m^2\ g^{-1}$ and an average pore diameter of approximately 15.1 nm. The material had its point of zero charge (PZC) determined (6.17) and its adsorption capacity was evaluated as a function of time, pH, and metal concentration. Dynamic adsorption equilibrium was reached in 120 min, and it had a good correlation with the pseudo-second-order kinetic model ($r^2 = 0.9997$). The maximum experimental adsorption capacity (0.0786 mmol g^{-1}) and the value calculated by the linearized Langmuir model (0.0799 mmol g^{-1}) are very approximate, indicating the formation of a monolayer over the material. Furthermore, the material proved to be very stable, because their adsorption capacity remained greater than 95% even after 10 cycles of adsorption/desorption. A high enrichment factor of 98.1-fold was observed, indicating that this material is suitable for the preconcentration of trace Cu(II) ions before analysis through flame atomic absorption spectrometry (FAAS).

1. Introduction

Copper is a microessential trace element and therefore plays important roles in the development and physiological processes of human beings and other organisms. As with any microessential element, copper is indispensable at a very narrow and low concentrations; however, at high concentrations, it can become very toxic, causing various health problems associated with the liver, bones, central nervous system, and the immune system [1,2]. On this basis, the development of analytical tools and artifices for the determination of trace metals in environmental or drinkable water sources/reservoirs is one of the main aims of the analytical chemistry, as they play an important role for the assessment of water quality, ultimately having a great effect over the health of humans and other organisms [3].

* Corresponding author at: Faculdade de Ciências Exatas e Tecnologia, Universidade Federal da Grande Dourados, Dourados, MS, Brazil.
E-mail address: marcoswondracek@gmail.com (M.H.P. Wondracek).

http://dx.doi.org/10.1016/j.apsusc.2016.01.172
0169-4332/

Recently, many modern instrumental techniques are used for the determination of heavy metals, such as electrochemical analysis, atomic absorption spectrometry (AAS) [4], atomic fluorescence spectrometry (AFS) [5], inductively coupled plasma optical emission spectrometry (ICP-OES) [6], and inductively coupled plasma mass spectrometry (ICP-MS) [7]. Among these, flame atomic absorption spectrometry (FAAS) is the most widely used due to the ease of operation as well as the low instrumental and operational costs [2]. Notwithstanding, the direct determination of metals in environmental samples by FAAS is often difficult due to matrix interferences and, most importantly, insufficient detection power of this technique [2,3]. Nevertheless, such difficulties could be overcome using preliminary preconcentration techniques before analysis through FAAS, which could extract the analytes from the matrix and increase their concentration in the samples, thus enabling their detection and quantification by such technique [3,8–11]. In view of this, various methods are proposed for the separation and preconcentration of metal ions from low concentration aqueous samples, such as cloud-point extraction, precipitation/coprecipitation, liquid–liquid extraction (LLE), and solid-phase extraction (SPE) [12,13]. With respect to SPE and LLE techniques, the first one has become the most popular because of its various advantages in comparison to LLE, such as production of less waste, reduced matrix effect, possibility of reuse of the solid phase, obtainment of higher enrichment factors, reduced consumption of organic solvents, possible coupling with different detectors, and because it is an environment-friendly technique [2,14–17]. On the contrary, the main disadvantage of SPE is the lack of selectivity, as it may be affected by the interference between coexisting metal species in the sample and the species of interest [18]. Thus, the development of new adsorbent materials aiming to increase sensitivity and selectivity in the determination of metal ions has gained special attention from the scientific community [15,19]. In this aspect, silica has been widely used as a solid support for the extraction of metals through SPE due to its hydrophilicity, the possibility of obtaining highly porous types of silica that can be synthesized through mild reactional routes (such as sol–gel), and the ease of chemically modifying its surface to obtain higher selectivity toward different analytes. For such reasons, many studies using chemically modified silica have already been reported [2].

On the contrary, due to some difficulties associated with the recovery and reutilization of materials applied in dispersive solid-phase microextraction (DSPME), such as material loss and/or long-lasting separation processes related to filtration steps, an appealing alternative to perform their extraction and recovery would consist of their magnetic separation, which could hypothetically simplify this process. The magnetic separation technique (MST) is based on the attraction force between a magnetic material and a magnetic field, but, as an important restriction, the material should not retain any residual magnetism as the field is removed. This means that the suspended magnetic material carrying the analyte of interest should readily be separated from a matrix by an external magnetic field without promoting the agglomeration of particles, as the magnetic field becomes null. As the main benefits of the application of magnetic separation, we could obtain a reduction of operational time, reduction of costs, and simplification of operational procedures, as it could prevent the use of SPE cartridges and peristaltic pumps. In view of this, nanoparticles of certain magnetic inorganic metal oxides appear to have suitable chemical and magnetic properties to be applied as magnetically extractable adsorbents, although their direct application is quite restricted because of their tendency to conglomerate and their poor selectivity. Nonetheless, if such particles could be coated by an appropriate shell, such restriction could be circumvented. Aiming to satisfy such condition, silica seems highly appealing in virtue of its many synthetic and chemical advantages already mentioned [20].

This work describes the synthesis of an ordered mesoporous Santa Barbara amorphous-type (SBA-15) silica with magnetic core of magnetite particles, its surface modification with the ligand 4-amino-3-hydrazino-5-mercapto-1,2,4-triazole (Purpald), and the results for the extraction of Cu(II) ions from aqueous medium through DSPME and SPE through column method. Parameters such as dynamic contact time, pH of the medium, and concentration of the analyte were studied. The materials produced were characterized through a series of techniques to verify the modification steps as well as to uncover the material's surficial properties to allow the assessment of its applicability as a potential adsorbent for metal ions. The characterization techniques consisted of magnetization measurements, scanning electron microscopy (SEM), high-resolution transmission electron microscopy (HR-TEM), Fourier transform infrared (FTIR), nuclear magnetic resonance (NMR) of ^{29}Si and ^{13}C, elemental analysis of carbon and nitrogen, determination of the point of zero charge (PZC), and surface area measurements.

2. Material and methods

2.1. Solvents, solutions, and reactants

All reagents were of high purity or at least of analytical grade. Aqueous solutions were prepared with high-purity deionized water whose resistivity indicated a value of 18.2 $M\Omega\,cm^{-1}$, collected from a Direct-Q system (Millipore, France). A Cu(II) stock solution (450 $mg\,L^{-1}$) was prepared by dissolving appropriate amounts of its nitrate salt (Sigma–Aldrich, USA) in deionized water. The following compounds were used for the synthesis of the magnetite particles: $FeCl_3$ (99%), $FeCl_2{\cdot}4H_2O$ (97%), and NH_4OH (28 wt.%). Moreover, nonionic surfactant triblock Pluronic (P123), tetraethoxysilane (TEOS; 99%), 3-chloropropyltriethoxysilane (CPTS; 95%), and Purpald (99%) were purchased from Sigma–Aldrich. The solutions used to build the calibration curves were prepared by an appropriate dilution of the stock standard solution (1000 $mg\,L^{-1}$) for atomic absorption analysis (Specsol). The pH of the solutions was adjusted with diluted HNO_3 (Carlos Erba) and NaOH (Sigma–Aldrich). All vessels were washed with HNO_3 (10%, v/v) for at least 24 h, rinsed with deionized water, and dried at room temperature before use.

2.2. Equipment

Modified silica-coated magnetic nanoparticles were characterized by infrared spectroscopy using an FTIR spectrometer (Nicolet Nexus 670; Thermo, USA). The materials were scanned 200 times at a resolution of 4 cm^{-1} through transmittance mode, and KBr pellets (200 mg) containing 1% in mass of the sample were prepared for this analysis. Specific surface area measurements were carried out in a Micromeritics ASAP2010 apparatus (Micromeritics Instrument Corp.) using 0.5 g material. Elemental analysis was performed using a Thermo Finnigan Flash 1112 Series EA CHN elemental analyzer with 2.0 mg of the materials. The quantification of Cu(II) was performed through an atomic absorption spectrometer operating in flame mode (AAnalyst 700; Perkin–Elmer, USA). SEM images were collected in a Quanta 200 SEM (FEI Co.) and HR-TEM images were collected in a JEM 2100 (Jeol, USA). The magnetic response of the selected nanocomposites was studied using a Quantum Design Magnetometer (VSM). High-resolution NMR spectra of the solid materials were obtained in an Agilent DD2 by applying a magnetic field of 5.9 T. The samples were packed in zirconium rotators of 4 mm in diameter. For the analyses of ^{13}C, rotation in magical angle spinning was applied with a frequency of 5 kHz

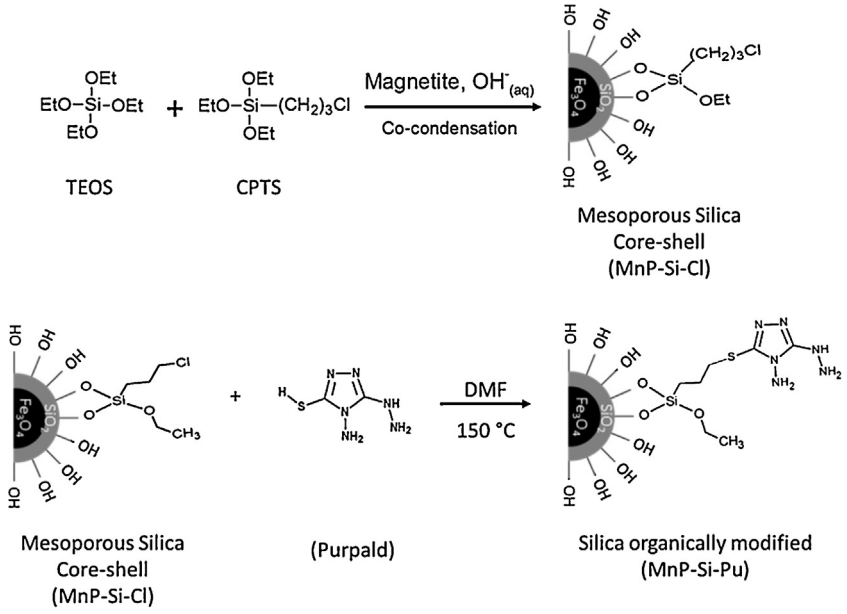

Fig. 1. Schematic representation of the main reaction steps occurring in the sol–gel process for the co-condensation method.

and cross-polarization (CP) $^{1}H \rightarrow {}^{13}C$. The Hartmann–Hahn contact time was 1 ms, and $\pi/2$ pulse of ^{1}H had a duration of 6 μs. During the acquisition of the ^{13}C signal, ^{1}H heteronuclear decoupling was applied with a nutation of 100 kHz. For each spectrum, 20,000 signals were collected for a duration of 5 s. The chemical deviation of ^{13}C was obtained in comparison with tetramethylsilane (TMS), using a solid sample of adamantane as a secondary standard, whose CH_2 resonance was observed in 38.6 ppm/TMS. In the analyses of ^{29}Si, an Hahn echo series of $\pi/2$-T_r-π with a pulse of $\pi/2$ of 7.5 μs, $T_r = 200$ μs (one period of rotation), and 14,800 acquisitions for a duration of 30 s were applied.

2.3. Synthesis of the silica-coated magnetite

Magnetite nanoparticles (MnPs) were prepared by a conventional coprecipitation method [20]. Briefly, 6.0 g $FeCl_3$ and 6.021 g $FeCl_2{\cdot}4H_2O$ g were dissolved in 111 mL deionized water. This mixture was heated to 80 °C and kept under nitrogen atmosphere under vigorous stirring. Then, 50 mL of 28% NH_4OH were added, and the color of the solution changed instantly from orange to black. The magnetite formed was washed thoroughly with deionized water until the pH of the suspension matched that of the water and then was stored in deionized high-purity water at a concentration of 35.5 g L^{-1}. Magnetic silica was prepared by the addition of 80 mL ultrapure water, 40 mL NH_4OH, and 4.0 g Pluronic into an Erlenmeyer flask. This mixture was heated to 40 °C under stirring until the complete dissolution of Pluronic. Then, 5.5 mL of the magnetite suspension (35.5 g L^{-1}), 5.0 mL TEOS, and 2.05 mL CPTS were added to the reaction flask and the mixture was stirred for 24 h. Afterwards, the mixture was transferred to a sealed vessel and aged in an oven at 100 °C for 24 h. The mixture was filtered and the material was dried, washed in a Sohxlet system (ethanol/water 1:1, v:v), ground, and stored in desiccator before use. The material produced in this step is called MnP–Si–Cl.

2.4. Functionalization of the material's surface

The modification of the material's surface was performed in a double-neck reaction flask. The mixture consisted of 20 mL dimethylformamide (DMF), 0.3359 g Purpald, and 0.5 mL triethylamine. The reagents were stirred and heated to 150 °C. After the dissolution of the Purpald, 0.6 g of the activated material MnP–Si–Cl was added to the reactional flask and the mixture was stirred for 72 h. Afterwards, the material was filtered under vacuum and washed in DMF at 100 °C for 30 min to remove the excess of ligand molecules. This procedure was repeated twice. The residue of DMF was removed by washing the material in a Soxhlet system for 24 h with an ethanol/water mixture (1:1). Finally, the material was dried at 50 °C for 24 h. Through this synthesis, a material named MnP–Si–Pu was produced. The synthesis steps are schematically shown in Fig. 1.

2.5. PZC experiment

To obtain more information about the surface of the material MnP–Si–Pu, an experiment to uncover its PZC was accomplished. In such experiment, 20.0 mg of this material were agitated with 10.0 mL of the solutions whose pH varied from 1 to 12. The solutions had their pH adjusted by the addition of HCl and NaOH solutions, and the material samples were agitated for 24 h before measuring the final pH [21].

2.6. Adsorption and reutilization experiments

Conventional batch experiments consisted of agitating 20.0 mg of the material with 1.80 mL of metal solution in 2 mL flasks. The material was later separated magnetically with the aid of a magnet, and the supernatant was collected to have its metal content analyzed via FAAS. Parameters such as contact time, pH, and analyte concentration were varied independently in each experiment. The contact times from 1 to 240 min were studied. The pH of the solutions was varied from 1 to 6, and the effect of the analyte concentration was investigated in the range from 1 to approximately 400 mg L^{-1}. The possibility of material reuse is also an interesting aspect, as it may be related to the reduction of costs and of the generated residues. In view of this, an experiment of cyclic adsorption and desorption was carried out to determine the physical and chemical stability of the synthesized material. This experiment was performed through cycles of percolation and elution in a packed column containing 40 mg MnP–Si–Pu. Then, 100 mL of the reference solutions of 0.10 mg L^{-1} were percolated through the column at flow rate of 2.5 mL min^{-1}, and metal elution was performed

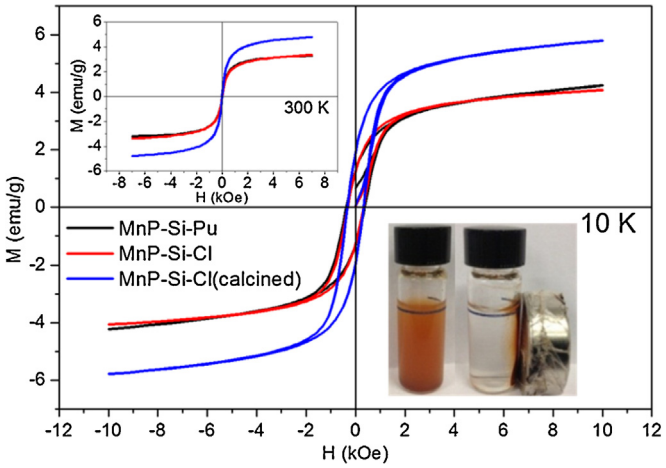

Fig. 2. Magnetization curve at 10 K for the calcined material [MnP–Si–Cl (calcined)], the chlorinated material (MnP–Si–Cl), and the material modified with the ligand molecule (MnP–Si–Pu). Top inset: Magnetization curve at 300 K. Bottom inset: Suspension of the material (MnP–Si–Pu) in aqueous medium before and after the application of an external magnetic field.

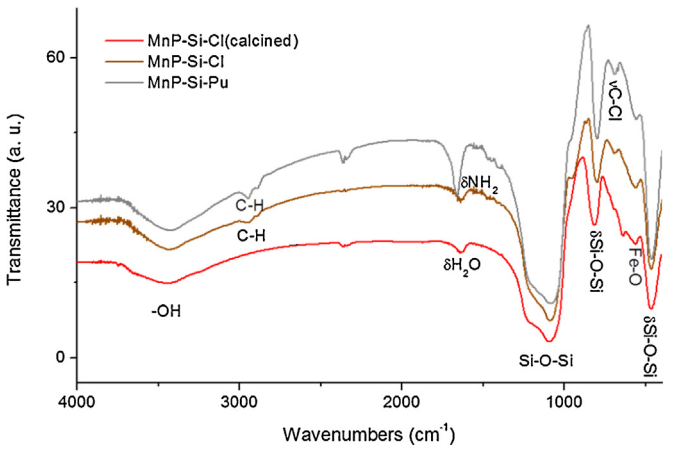

Fig. 3. Infrared spectra of the calcined mesoporous silica [MnP–Si–Cl (calcined)], the silylated mesoporous silica (MnP–Si–Cl), and the mesoporous silica modified with ligand (MnP–Si–Pu).

with 1.0 mL eluent (a solution composed of 1.0 mol L^{-1} HCl and 0.2 mol L^{-1} thiourea) at a flow rate of 1.0 mL min^{-1}. The eluate was collected and subjected to FAAS analysis. All experiments were accomplished at room temperature (approximately 25 °C).

3. Results and discussion

3.1. Characterization of the materials

The material had its magnetic properties evaluated and the results are visually presented in Fig. 2. This figure shows the measurements of magnetization versus magnetic induction accomplished at 10 and 300 K for the materials obtained at different stages of the synthesis. At 10 K, hysteresis could be observed for all the materials, which indicates that, at such temperature, the materials preserve a remnant magnetization, even when the magnetic induction is null. It is also possible to observe a decrease in the values of magnetization in comparison with the calcined material, as the chemical modification of the material's surface is carried out, which is due to the presence of the organic content in the surface of the material. At 300 K (Fig. 2, inset), the hysteresis phenomenon does not occur (superparamagnetic materials) because, with the increase in the temperature, the thermal energy becomes similar or larger than the anisotropy energy, allowing the magnetic moment of the particles to vary in orientation; in other words, the material cannot maintain spontaneous magnetization at temperatures close to the ambient temperaure, and this favors its stability as a colloidal suspension in liquid media. As an external magnetic field is applied, the material will have a high magnetization, and as soon as the field is removed, it will return to its initial condition with an extremely small relaxation time. In view of this, the magnetic separation of the composite in a liquid phase can be performed rapidly by approaching a magnet to the vessel containing the suspended material, as demonstrated in Fig. 2(inset).

The results of the elemental analysis are shown in Table 1. These data show the percentile differences in the carbon and nitrogen content for each synthetic step, indicating the variation of the organic moieties. The material synthesized by the co-condensation method, called MnP–Si–Cl, has a high concentration of carbon, which indicates that the silylating agent (CPTS) is anchored to it. The increase in nitrogen and carbon contents for MnP–Si–Pu indicates that the reaction with Purpald is probably successful. It is also noted that the increase in the nitrogen content is significantly higher than that of carbon. This result is expected because the Purpald molecule contains three nitrogen atoms for each of its carbon atoms. From these results, the ratio of ligand in the organofunctionalized material is 0.3 mmol g^{-1}.

Table 1
Elemental analysis of the material in the two-step synthesis.

Sample	C (%)	N (%)
MnP–Si–Cl	11.6	1.15
MnP–Si–Pu	12.2	4.0

FTIR spectroscopy was used to determine the functional groups of the modified nanoparticles as well as the occurrence of each modification step. Therefore, infrared spectra were collected for the MnP–Si–Cl (calcined), MnP–Si–Cl, and MnP–Si–Pu materials (Fig. 3). The broad band of approximately 3400 cm^{-1} is usually assigned to νO–H, SiO–H vibration, and/or adsorbed water [22,23]. Other charateristic silica absorption bands were also observed in the region of 1100 cm^{-1}, which are related to νSi–O–Si stretching vibrations, and at 805 and 457 cm^{-1}, corresponding to δSi–O–Si bending vibrations [22,24]. By comparing MnP–Si–Cl (calcined) with the chlorinated silica spectrum (MnP–Si–Cl), the reaction between TEOS and the silylating agent (CPTS) is probably successful, as three bands at 2950, 645, and 698 cm^{-1} could be noticed. These bands may be respectively assigned to the stretching vibration of νC–H, CH_2–Si, and νC–Cl bonds from the structure of CPTS [22]. It is still possible to observe in the spectrum of the calcined silica and MnP–Si–Cl a weak band of approximately 560 cm^{-1}, characteristic of Fe–O vibrations from the magnetite core [24]. The spectrum of MnP–Si–Pu has two main differences in comparison to the spectrum of the chlorinated silica; the absorption band located at 1635 cm^{-1} (for the chlorinated silica) is shifted to a higher wavenumber (1660 cm^{-1}) and also became more intense. This band not only corresponds to bending vibrations of $\delta(H_2O)$ but could also be attributed to the amino groups $\delta(NH_2)$ [25] of the ligand molecule.

The FTIR results obtained indicated that the reaction of organofunctionalization probably occurred, although a more profound investigation through ^{29}Si and ^{13}C NMR analysis was carried out to either confirm or disprove them. Regarding the NMR analysis for ^{29}Si Fig. 4, we can notice resonances corresponding to SiO_4 species of type Q^4 (−105 ppm) and groups $(SiO)_2Si^*(OCH_3)$(D) (−62 ppm) and T $(SiO)_3Si^*C$ (−73 ppm), which were identified specifically as D and T. This result demonstrates that silica domains are highly connected, with no significant amount of less connected

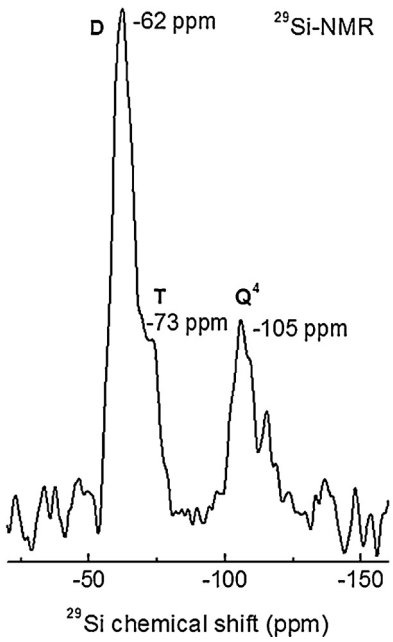

Fig. 4. NMR spectrum of ^{29}Si of the material MnP–Si–Pu.

Q^3 groups and with groups T and D in the surface. Yet, based on the NMR analyses of ^{13}C for the materials MnP–Si–Pu and MnP–Si–Cl, Fig. 9 and Table 3 were built. In Table 2, we can find the chemical deviations of the observed resonances as well as to which chemical groups they were attributed. As seen in Table 2, C–Si, CH_2, C–Cl, and OCH_3 were common groups for both materials and these resonances are implied in the presence of CPTS in the surface of these modified materials. Nonetheless, C—S bonds could only be detected for the material MnP–Si–Pu, which indicates the coupling of the Purpald molecule to this material's surface through its sulfhydryl group. In Fig. 5, both spectra present the same resonance groups, except for the region comprehended between 30 and 50 ppm. With respect to the spectrum of the material MnP–Si–Cl, an intense resonance at 45.3 ppm corresponding to the C—Cl bond was found, whereas, for the material MnP–Si–Pu, this same resonance was reduced and a new resonance at 35.8 ppm can be clearly seen, which was associated with C—S groups. Such observations may indicate the rupture of the C—Cl bonds to give place to C—S bonds between the material's surface and the ligand, ultimately indicating the occurrence of the functionalization step.

To assess the surface properties of the produced materials, such as specific surface area and average pore size, surface area measurements using nitrogen gas were performed. The nitrogen isotherms of the materials, in the different stages of synthesis, indicated type IV adsorption isotherms with hysteresis between the adsorption

Table 2
Chemical deviations of the resonances obtained for ^{13}C of the materials MnP–Si–Pu and MnP–Si–Cl.

MnP–Si–Cl ^{13}C–δ_{iso} (ppm)	MnP–Si–Pu ^{13}C–δ_{iso} (ppm)	Attribution
4.3	5.2	
8.6	9.7	C–Si
15.0	13.7	
24.9	22.5	CH_2
Absent	35.8	C–S
45.3	45.0	C–Cl
56.0	54.0	
62.6	62.4	OCH_3
69.0	69.3	

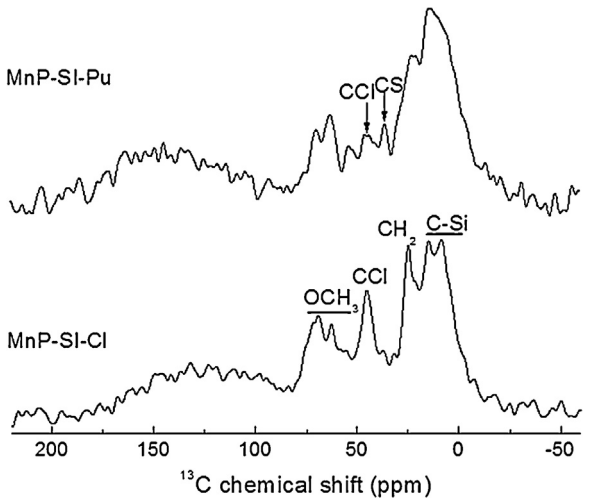

Fig. 5. NMR spectrum (magical angle spinning) of ^{13}C of the materials MnP–Si–Cl and MnP–Si–Pu.

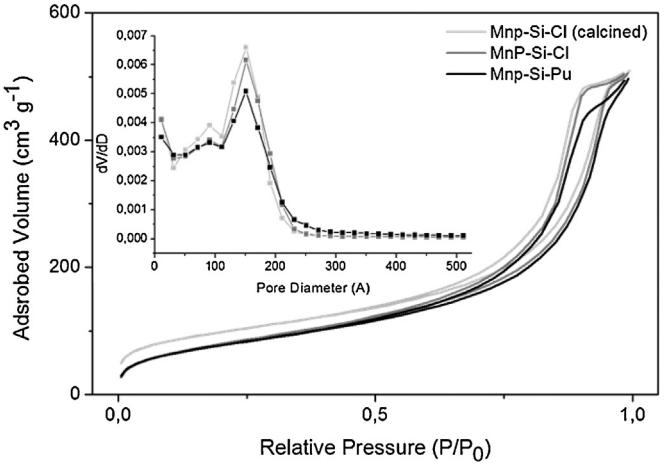

Fig. 6. Nitrogen adsorption isotherms and average pore diameter for calcined mesoporous silica [MnP–Si–Cl (calcined)], the silylated mesoporous silica (MnP–Si–Cl), and the mesoporous silica modified with ligand (MnP–Si–Pu).

and desorption branches, as shown in Fig. 6, which are characteristic for mesoporous materials presenting capillary condensation inside the pores [26]. Yet, the type of the hysteresis noted between the adsorption–desorption isotherms of Fig. 6 is classified as H1. The relative pressure range where this phenomenon occurs, as well as its format, depends mainly on the geometry of the pores, and the H1-type hysteresis is observed in regular mesoporous solids with cylindrical and/or polyhedral format with open ends [27]. Moreover, the material presented an average pore diameter of 151 Å, comprehended in a range from 31 to 210 Å (Fig. 6, inset). The specific surface area and pore volume of the materials produced in each step of the synthesis are found in Table 3. The obtained values for the surface area of the materials are inversely proportional to the amount of organic molecules attached to the material, as the molecules grafted onto silica's surface occupy partially the pores of

Table 3
Pore structure parameters of the material in different stages of functionalization.

Sample	S_{BET} ($m^2\ g^{-1}$)	V_{BJH} ($cm^3\ g^{-1}$)
MnP–Si–Cl (calcined)	354.93 ± 0.76	0.770990
MnP–Si–Cl	298.85 ± 1.22	0.758001
MnP–Si–Pu	287.99 ± 0.81	0.731418

S_{BET}, specific area; V_{BJH}, mean pore volume.

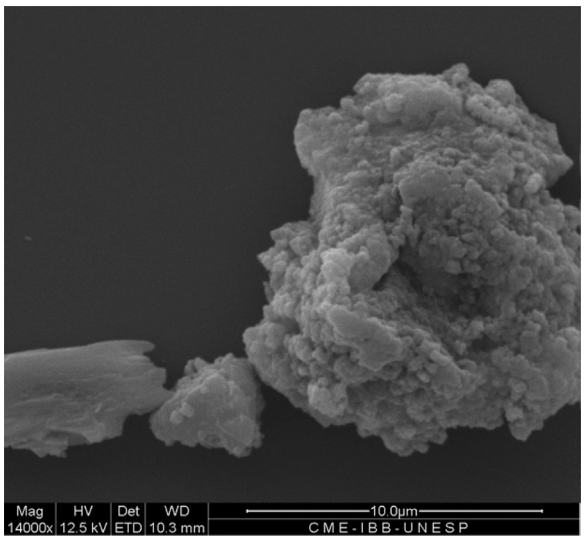

Fig. 7. SEM images for the MnP–Si–Pu material.

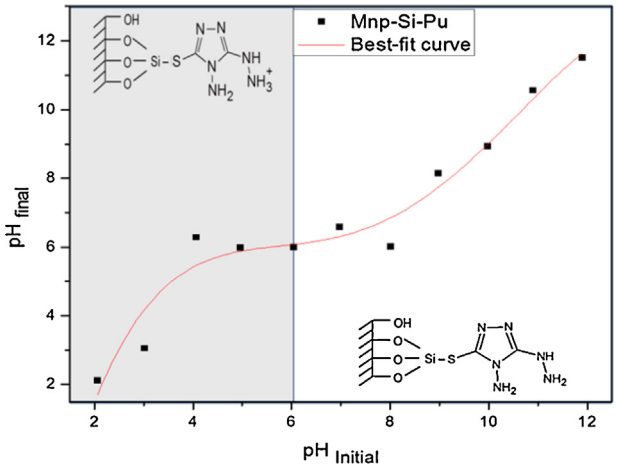

Fig. 9. Determination of the pH of the PZC and representation of the charges on the material's surface at different pHs.

the material, blocking them; thus, a reduction in the surface area and pore volume is expected after the organofunctionalization [17], as seen in Table 3. The average pore diameter values obtained are within the range of 2.0–50.0 nm, which are in the range specified for mesoporous materials, thus corroborating with the isotherm type provided by the adsorption and desorption of nitrogen.

The morphology of the silica could be obtained through SEM, as seen in Fig. 7. In this figure, the particles of the material do not have a regular form but are quite porous and their surface is very rough. These features, which are associated with a small particle diameter (approximately 10 μm), implies that the material presents a high surface area and consequently a large contact surface (as already estimated by surface area measurements), which is interesting for adsorbent materials.

Fig. 8 shows the HR-TEM images of the material MnP–Si–Pu. In Fig. 8a, it is possible to observe different electron densities along the image. The darker regions are associated with the magnetic nanoparticles, whereas the lighter regions are associated with the silica coating, as demonstrated by the arrows. These observations could be confirmed in Fig. 8b as well, because, as we zoom in to the dark regions (rectangles specified as 1 and 2), it is possible to observe an interfringe spacing, characteristic of organized atomic arrangements of crystal structures that are commonly observed for iron oxides, such as magnetite [28]. In addition, such patterns could not be assigned to the silica shell because the atomic structure of silica is amorphous and therefore cannot provide a regular electron scattering. In view of this, mesoporous silica could indeed be deposited on the surface of the magnetite particles, as desired.

Finally, before the application of the modified material in adsorption experiments, an investigation to uncover its PZC was carried out. This experiment is very important to understand adsorption processes, as it provides information about the surficial charge as a function of the pH of the medium and thus allow making predictions about at which pH values such processes are favorable or unfavorable. Depending on the pH of the medium, the surface can be positively, negatively, or even neutraly charged. For the case of the resultant charge to be null, we have the condition of PZC, which was represented by pH_{PZC}. As the pH of the medium increases above pH_{PZC} ($pH > pH_{PZC}$), the material's surface acquires a resultant negative charge mainly due to phenomena such as deprotonation of surficial groups and/or adsorption of hydroxyl species. On the contrary, if the pH of the medium is below pH_{PZC} ($pH < pH_{PZC}$), the material's surface will be positively charged, which is due to the protonation of such surfical groups [29]. The data collected from the PZC experiment were used to build Fig. 9, and the pH_{PZC} was calculated as the average of the final pH values measured in the range in which such values remained almost contant. From these results, the pH_{PZC} of the material MnP–Si–Pu was 6.2.

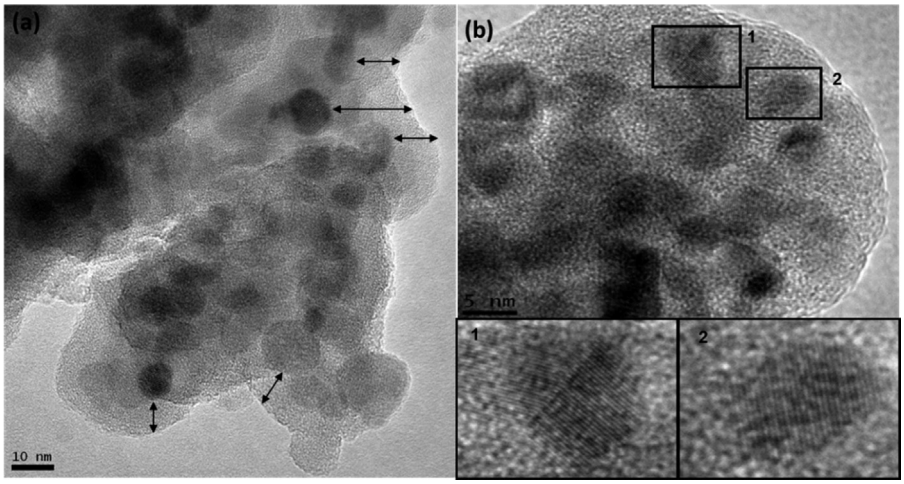

Fig. 8. HR-TEM images for the MnP–Si–Pu material: (a) normal image and (b) application of zoom in demarcated areas.

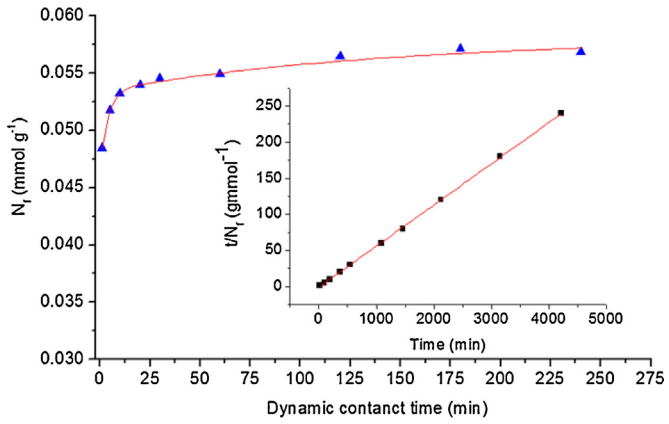

Fig. 10. Kinetic study for the adsorption of copper onto the surface of MnP–Si–Pu.

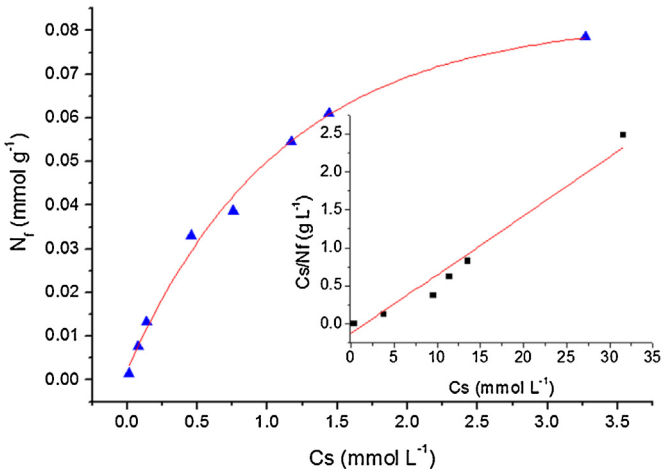

Fig. 11. Adsorption isotherm for Cu(II) in aqueous medium for modified silica and its linear form according to Langmuir model (embedded).

3.2. Experiments of Cu(II) extraction in batch mode

Relevant parameters were investigated to characterize the obtained material regarding its adsorption properties, such as adsoption kinetics, influence of pH, and maximum adsorption capacity.

The adsorption capacity for each condition was obtained by comparing the metal content in the solution before and after the experiments. Eq. (1) was used to calculate the amount of retained metal ions per gram of material (N_f):

$$N_f = \frac{n_i - n_s}{m}, \quad (1)$$

where n_i is the amount of metal ions (mmol) in the initial solution, n_s is the amount of metal ions (mmol) in the supernatant, and m is the mass of the material used (g).

The influence of pH in the adsorption of Cu(II) over the material's surface was investigated in the range from 1 to 6 to uncover the optimized pH condition. The experiments were conducted with 1.8 mL aqueous Cu(II) solutions in the concentration of 50 mg L^{-1}. The results indicated that the adsorption capacity was stabilized at pH 2, suggesting that, even in pH values lower than pH_{PZC}, the material's surface is favorable for the adsorption of Cu(II). This property is interesting, as it enables the removal of Cu(II) from acidic residues.

The dynamic contact time is another important aspect regarding adsorption processes. In this work, the contact time was investigated in a range from 1 to 240 min. In Fig. 10, the equilibrium was reached at approximately 120 min. The red curve representing the adsorption isotherm indicates two equilibrium stages, which may be explained by metal adsorption over readily available sites followed by a subsequent adsorption over more internal sites (with some steric hindrance).

To better understand Cu(II) adsorption kinetics of MnP–Si–Pu, mathematical kinetic models such as the pseudo-first-order and pseudo-second-order kinetic models [30,31] were applied to the experimental data. The pseudo-first-order kinetic model is expressed in Eq. (2):

$$\mathrm{Log}\,(q_e - q_t) = \mathrm{Log}(q_e) - \frac{k_1 t}{2.303}, \quad (2)$$

where q_e and q_t are the adsorption capacities for the metal ions (mg g^{-1}) in equilibrium and at time t (min), respectively, and k_1 (min^{-1}) is the kinetic constant of this model. Calculated q_e and k_1 can be both obtained from the intercept and the slope when we plot $\log(q_e - q_t)$ versus t. The determination coefficient obtained for the pseudo-first-order kinetic model was very low ($r^2 = 0.838$). Furthermore, the calculated q_e (=0.0057 mmol g^{-1}) and the experimental q_e observed from the isotherm in Fig. 10 are not in agreement, which indicates that such model is not representative for the kinetic adsoptive behavior of MnP–Si–Pu toward Cu(II) ions. In spite of this, the adsorption kinetics of the material could be well described by the pseudo-second-order kinetic model, as expressed by Eq. (3):

$$\frac{t}{N_{ft}} = \frac{1}{KN_f^2} + \frac{1}{N_f}t, \quad (3)$$

where N_{ft} is the adsorption capacity at a given time (mmol g^{-1}), N_f is the adsorption capacity at equilibrium (mmol g^{-1}), K is the kinetic constant of the pseudo-second-order model (mmol g^{-1} min^{-1}), and t is the contact time for each experiment (min). By plotting the values of t/N_{ft} versus t, it was possible to obtain the straight line represented in Fig. 10(inset), whose determination coefficient (r^2) was found to be 0.9997. Moreover, N_f provided 0.057 mmol g^{-1}, whereas K provided 14.60 mmol g^{-1} min^{-1}. The determination coefficient indicates that the pseudo-second-order model better represents the adsorption process of MnP–Si–Pu and that the kinetic adsorption mechanism toward Cu(II) is determined by a chemical interaction. This implies that free-electron pairs existing on the surface of the material are being shared with metal species in solution by means of covalent bonds [32]. In addition, the good correlation of the data with such model may also be verified through the agreement between the calculated N_f and the experimental N_f observed in the adsorption isotherm of Fig. 10.

Experiments to determine the maximum adsorption capacity were also performed in batch mode, making use of the optimized parameters from pH and contact time experiments and by varying Cu(II) concentration. As we plot N_f values versus the respective supernatant concentrations (C_s), we can build the adsorption isotherm depicted in Fig. 11. In Fig. 11, it is possible to infer that the experimental maximum adsorption is approximately 0.080 mmol g^{-1}. The collected data were also applied to Langmuir and Freundlich linearized models. The Langmuir model assumes that the energy of the adsorption sites is identical and that one adsorbate occupies only a single site, resulting in the formation of a monolayer over the adsorbent's surface [34]. The maximum amount of Cu(II) adsorbed onto the material's surface, N_s (mmol g^{-1}), at equilibrium may be calculated through the linearized Langmuir equation [Eq. (4)]:

$$\frac{C_s}{N_f} = \frac{C_s}{N_s} + \frac{1}{bN_s}, \quad (4)$$

where C_s is the supernatant concentration at equilibrium (mmol L^{-1}), N_f is the adsorption capacity of metal ions on the material's surface for a given concentration (mmol g^{-1}), and b is a constant related to the affinity between adsorbate and the

Table 4
Comparison between the maximum adsorption capacities of the material produced in that study and other adsorbent materials.

Adsorbent	Adsorption capacity Cu (II) (mmol g^{-1})	References
Brazilian Orchid Tree	0.140	[33]
Silica-supportedbis(diazoimine)	0.003	[34]
Nano-TiO_2 modified with 2-mercaptobenzothiazole	0.062	[35]
Untreated coffee husks	0.118	[36]
Uncaria gambir	0.156	[37]
Commercial Coffee Wastes	1.101	[38]
Corn Leaf Powder	0.089	[39]
Silica Functionalized	0.012	[40]
p-Morpholinomethylcalix[4]arene bonded silica	0.026	[41]
Calcium-alginate-modified diethylenetriamine-silica gel	0.123	[42]
Multi-carboxyl-functionalized silica gel	0.740	[43]
Silica on multi-walled carbon nanotubes	1.047	[44]
Silica sequentially modified with polyhexamethylene guanidine and Arsenazo	0.060	[45]
Amidoamidoxime silica	0.016	[2]
Silica modified with chlorodimethylvinylsilane	0.020	[46]
Silica-coated magnetite, core–shell, modified with purpald	0.079	This study

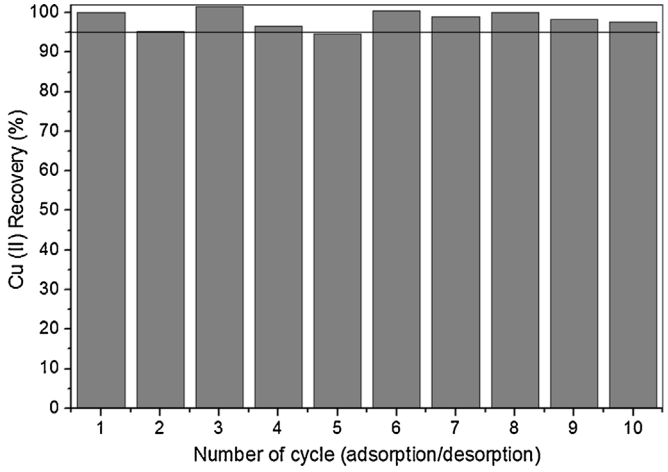

Fig. 12. Column reutilization experiment, Cu(II) recovery after 10 adsorption/desorption cycles.

binding sites (L $mmol^{-1}$). The correlations obtained by the application of Langmuir model were satisfactory and indicated that adsorption process may be occurring through the formation of a monolayer, as N_s (=0.0799 mmol g^{-1}) is very close to the N_f at the highest concentration of Cu(II) (0.0786 mmol g^{-1}), and the determination coefficient (r^2) is considerably high (0.9686).

The linearized Freundlich adsorption model was also used to interpret the data, as expressed in Eq. (5):

$$\log N_f = \log K_f + \frac{1}{n} \log C_s, \quad (5)$$

where K_f and n are constants related to the Freundlich adsorption capacity and adsorption intensity, respectively [32]. From such equation, the calculated K_f was 1.064 mmol g^{-1} and the determination coefficient (r^2) was 0.876. Comparing both mathematical adsorption models, the Langmuir best described the adsorption process for the system studied. According to several studies listed in Table 4, the maximum adsorption capacity of MnP–Si–Pu is similar compared to other adsorbents. Moreover, besides the simple synthetic preparation of MnP–Si–Pu, the reutilization experiments accomplished in packed columns provided that this material is stable for a minimum of 10 adsorption/desorption cycles with recoveries above 98% (Fig. 12). Yet, reutilization experiments provided an enrichment factor of approximately 98-fold, which indicates that the material presents a great potential for analytical preconcentration procedures.

4. Conclusion

The synthesis procedure is very simple, and and the coating of MnPs with a mixture of TEOS and CPTS results in a magnetically extractable silica-based material suitable for organofunctionalization. The characterization of the organofunctionalized material through different techniques confirmed the presence of the ligand on the surface of the material and that the reaction occurred through the sulfydryl group of the ligand to give place to a C—S bond. The obtained material consists of mesoporous particles of irregular shapes, presenting rough surface with a relatively high surface area. The surficial properties indicated that the material is suitable to perform adsorption of metal ions from aqueous media, as confirmed through the adsorption experiments. The material demonstrated to be efficient in the uptake of Cu(II) ions in a large pH range (2–6) and very physically and chemically stable even after undergoing adsorption/desorption cycles (it may be used for at least 10 cycles without loss in its adsorption capacity). Moreover, the high enrichment factor obtained (98-fold) indicates that it could be applied for analytical purposes, such as the preconcentration and determination of trace amount of Cu(II) in aqueous media.

Acknowledgments

The authors thank Fundacão de Amparo à Pesquisa do Estado de São Paulo (FAPESP; Proc: 2012/21795-9, 2015/04791-8, 2015/05224-0, and 2013/22955-2), CNPq (Proc: 302284/2012-5), and Universidade Federal da Grande Dourados (UFGD) for the fellowship granted to M.H.P. Wondracek during the execution of this study. The authors also thank the Centro de Microscopia Eletrônica (CME) of the Institute of Biosciences of Unesp (Botucatu) and the Microscopy Laboratory of IPEN.

References

[1] A.M. Ghaedi, M. Ghaedi, A. Vafaei, N. Iravani, M. Keshavarz, M. Rad, I. Tyagi, S. Agarwal, V.K. Gupta, Adsorption of copper(II) using modified activated carbon prepared from pomegranate wood: optimization by bee algorithm and response surface methodology, J. Mol. Liq. 206 (2015) 195–206.
[2] W. Ngeontae, W. Aeungmaitrepirom, T. Tuntulani, A. Imyim, Highly selective preconcentration of Cu(II) from seawater and water samples using amidoamidoxime silica, Talanta 78 (2009) 1004–1010.
[3] M. Ghaedi, F. Ahmadi, M. Soylak, Preconcentration and separation of nickel, copper and cobalt using solid phase extraction and their determination in some real samples, J. Hazar. Mater. 147 (2007) 226–231.
[4] G.K. Tasneem, M.K. Jamali, M.B. Arain, H.I. Afridi, N. Jalbani, R.A. Sarfraz, R. Ansari, Evaluation of an ultrasonic acid digestion procedure for total heavy metals determination in environmental and biological samples, J. Hazard. Mater. 161 (2009) 1391–1398.
[5] J.L. Gómez-Ariza, D. Sánchez-Rodas, I. Giráldez, E. Morales, A comparison between ICP-MS and AFS detection for arsenic speciation in environmental samples, Talanta 51 (2000) 257–268.
[6] V. Chand, S. Prasad, ICP-OES assessment of heavy metal contamination in tropical marine sediments: a comparative study of two digestion techniques, Microchem. J. 111 (2013) 53–61.
[7] F.J.S. López, M.D.G. Garcia, N.P.S. Morito, J.L.M. Vidal, Determination of heavy metals in crayfish by ICP-MS with a microwave-assisted digestion treatment, Ecotox. Environ. Saf. 54 (2003) 223–228.
[8] H. Bagheri, A. Afkhami, M. Saber-Tehrani, H. Khoshsafar, Preparation and characterization of magnetic nanocomposite of Schiff base/silica/magnetite as a preconcentration phase for the trace determination of heavy metal ions in water, food and biological samples using atomic absorption spectrometry, Talanta 97 (2012) 87–95.

[9] M. Soylak, Y.E. Unsal, Chromium and iron determinations in food and herbal plant samples by atomic absorption spectrometry after solid phase extraction on single-walled carbon nanotubes (SWCNTs) disk, Food Chem. Toxicol. 48 (2010) 1511–1515.
[10] Y. Wang, T. Tian, L. Wang, X. Hu, Solid-phase preconcentration of cadmium(II) using amino-functionalized magnetic-core silica-shell nanoparticles, and its determination by hydride generation atomic fluorescence spectrometry, Microchim. Acta 180 (2013) 235–242.
[11] C.H. Latorre, J.Á. Méndez, J.B. García, S.G. Martín, R.M.P. Crecente, Carbon nanotubes as solid-phase extraction sorbents prior to atomic spectrometric determination of metal species: a review, Anal. Chim. Acta 749 (2012) 16–35.
[12] M.H. Mashhadizadeh, Z. Karami, Solid phase extraction of trace amounts of Ag, Cd, Cu, and Zn in environmental samples using magnetic nanoparticles coated by 3-(trimethoxysilyl)-1-propantiol and modified with 2-amino-5-mercapto-1,3,4-thiadiazole and their determination by ICP-OES, J. Hazard. Mater. 190 (2011) 1023–1029.
[13] J.S. Suleiman, B. Hu, H. Peng, C. Huang, Separation/preconcentration of trace amounts of Cr, Cu and Pb in environmental samples by magnetic solid-phase extraction with Bismuthiol-II-immobilized magnetic nanoparticles and their determination by ICP-OES, Talanta 77 (2009) 1579–1583.
[14] M. Ghaedi, H. Tavallali, A. Shokrollahi, M. Zahedi, M. Montazerozohori, M. Soylak, Flame atomic absorption spectrometric determination of zinc, nickel, iron and lead in different matrixes after solid phase extraction on sodium dodecyl sulfate (SDS)-coated alumina as their bis (2-hydroxyacetophenone)-1,3-propanediimine chelates, J. Hazard. Mater. 166 (2009) 1441–1448.
[15] G. Xiang, L. Li, X. Jiang, L. He, L. Fan, Thiol-modified magnetic silica sorbent for the determination of trace mercury in environmental water samples coupled with cold vapor atomic absorption spectrometry, Anal. Lett. 46 (2013) 706–716.
[16] X. Huang, X. Chang, Q. He, Y. Cui, Y. Zhai, N. Jiang, Tris(2-aminoethyl) amine functionalized silica gel for solid-phase extraction and preconcentration of Cr(III), Cd(II) and Pb(II) from waters, J. Hazard. Mater. 157 (2008) 154–160.
[17] R.K. Sharma, A. Pandey, S. Gulati, A. Adholeya, An optimized procedure for preconcentration, determination and on-line recovery of palladium using highly selective diphenyldiketone-monothiosemicarbazone modified silica gel, J. Hazard. Mater. 209–210 (2012) 285–292.
[18] W. Ngeontae, W. Aeungmaitrepirom, T. Tuntulani, Chemically modified silica gel with aminothioamidoanthraquinone for solid phase extraction and preconcentration of Pb(II), Cu(II), Ni(II), Co(II) and Cd(II), Talanta 71 (2007) 1075–1082.
[19] M.H. Mashhadizadeh, M. Amoli-Divaa, Atomic absorption spectrometric determination of Al^{3+} and Cr^{3+} after preconcentration and separation on 3-mercaptopropionic acid modified silica coated-Fe_3O_4 nanoparticles, J. Anal. At. Spectrom. 28 (2013) 251–258.
[20] C. Huang, W. Xie, X. Li, J. Zhang, Speciation of inorganic arsenic in environmental waters using magnetic solid phase extraction and preconcentration followed by ICP-MS, Microchim. Acta 173 (2011) 165–172.
[21] W.F. Tan, S.J. Lu, F. Liu, X.H.J. Feng, Z. He, L.K. Koopal, Determination of the point of zero charge of manganese oxides with different methods including and improved salt, Soil Sci. 173 (2008) 277–286.
[22] F. Adam, H. Osman, K.M. Hello, The immobilization of 3-(chloropropyl)triethoxysilane onto silica by a simple one-pot synthesis, J. Colloid Interface Sci. 331 (2009) 143–147.
[23] S.M. Evangelista, E. de Oliveira, G.R. Castro, L.F. Zara, A.G.S. Prado, Hexagonal mesoporous silica modified with 2-mercaptothiazoline for removing mercury from water solution, Surf. Sci. 601 (2007) 2194–2202.
[24] C. Birsan, D. Predoi, E. Andronescu, IR and thermal studies of iron oxide nanoparticles in a bioceramic matrix, J. Optoelectron. Adv. Mater. 9 (2007) 1821–1824.
[25] R. Dobrowolski, M. Oszust-Cieniuch, J. Dobrzyńska, M. Barczak, Amino-functionalized SBA-15 mesoporous silicas as sorbents of platinum(IV) ions, Colloids Surf. A. 435 (2013) 63–70.
[26] K.S.W. Sing, D.H. Everett, R.A.W. Haul, L. Moscou, R.A. Pierotti, J. Rouquerol, T. Siemieniewska, Reporting physisorption data for gas/solid systems with special reference to the determination of surface area and porosity, Pure Appl. Chem. 57 (1985) 603–619.
[27] J.H.G. Rangel, H.C.C. dos Santos, M.M. Oliveira, E. Longo, Síntese e caracterização estrutura de SNO_2 dopado com Ni, HOLOS 4 (2011) 112–127.
[28] E. Delahaye, V. Escax, N. El Hassan, A. Davidson, R. Aquino, V. Dupuis, R. Perzynski, Y.L. Raikher, "Nanocasting": using SBA-15 silicas as hard templates to obtain ultrasmall monodispersed γ-Fe_2O_3 nanoparticles, J. Phys. Chem. B 110 (2006) 26001–26011.
[29] A.O. Jorgetto, R.I.V. Silva, M.J. Saeki, R.C. Barbosa, M.A.U. Martines, S.M.A. Jorge, A.C.P. Silva, J.F. Schneider, G.R. Castro, Cassava root husks powder as green adsorbent for the removal of Cu(II) from natural river water, Appl. Surf. Sci. 288 (2014) 356–362.
[30] Y.S. Ho, G. McKay, Pseudo-second order model for sorption processes, Process Biochem. 34 (1999) 451–465.
[31] S. Lagergren, About the theory of so-called adsorption of soluble substances, K. Sven. Vetenskapsakad. Handl. 24 (1898) 1–39.
[32] N. Feng, X. Guo, S. Liang, Adsorption study of copper(II) by chemically modified orange peel, J. Hazard. Mater. 164 (2009) 1286–1292.
[33] A.O. Jorgetto, A.C.P. da Silva, M.H.P. Wondracek, R.I.V. Silva, E.D. Velini, M.J. Saeki, V.A. Pedrosa, G.R. Castro, Multilayer adsorption of Cu(II) and Cd(II) over Brazilian Orchid Tree (Pata-de-vaca) and its adsorptive properties, Appl. Surf. Sci. 345 (2015) 81–89.
[34] S. Uruş, S. Purtaş, G. Ceyhan, F. Tümer, Solid phase extraction of Pb(II), Cu(II), Cd(II) and Cr(III) with syringe technique using novel silica-supported bis(diazoimine) ligands, Chem. Eng. J. 220 (2013) 420–430.
[35] N. Pourreza, S. Rastegarzadeh, A. Larki, Simultaneous preconcentration of Cd(II), Cu(II) and Pb(II) on Nano-TiO_2 modified with 2-mercaptobenzothiazole prior to flame atomic absorption spectrometric determination, J. Ind. Eng. Chem. 20 (2014) 2680–2686.
[36] W.E. Oliveira, A.S. Franca, L.S. Oliveira, S.D. Rocha, Untreated coffee husks as biosorbents for the removal of heavy metals from aqueous solutions, J. Hazard. Mater. 152 (2008) 1073–1081.
[37] K.S. Tong, M.J. Kassim, A. Azraa, Adsorption of copper ion from its aqueous solution by a novel biosorbent *Uncaria gambir*: equilibrium, kinetics, and thermodynamic studies, Chem. Eng. J. 170 (2011) 145–153.
[38] G.Z. Kyzas, Commercial coffee wastes as materials for adsorption of heavy metals from aqueous solutions, Materials 5 (2012) 1826–1840.
[39] A.C.P. Silva, A.O. Jorgetto, M.H.P. Wondracek, M.J. Saeki, J.F. Schneider, V.A. Pedrosa, M.A.U. Martines, G.R. Castro, Characterization of corn (Zea mays) leaf powder and its adsorption properties reagarding Cu(II) and Cd(II) from aqueous samples, Bioresources 10 (2015) 1099–1114.
[40] A.O. Jorgetto, S.P. Pereira, R.I.V. Silva, M.J. Saeki, M.A.U. Martines, V.A. Pedrosa, G.R. Castro, Application of mesoporous SBA-15 silica functionalized with 4-amino-2-mercaptopyrimidine for the adsorption of Cu(II), Zn(II), Cd(II), Ni(II), and Pb(II) from water, Acta Chim. Slov. 62 (2015) 111–121.
[41] F.N. Memon, H.F. Ayyilidiz, H. Kara, S. Memon, A. Kenar, M.K. Leghari, M. Topkafa, S.T.H. Sherazi, N.A. Memon, F. Durmaz, I. Tarhan, Application of central composite design for the optimization of on-line solid phase extraction of Cu^{2+} by calix[4]arene bonded silica resin, Chemometr. Intell. Lab. 146 (2015) 158–168.
[42] M. Mori, T. Suzuki, T. Sugita, D. Nagai, K. Hirayama, M. Onozato, H. Itabashi, Heavy metal adsorptivity of calcium-alginate-modified diethylenetriamine–silica gel and its application to a flow analytical system using flame atomic absorption spectrometry, Anal. Chim. Acta 840 (2014) 42–48.
[43] M. Li, M. Li, C. Feng, Q. Zeng, Preparation and characterization of multi-carboxyl-functionalized silica gel for removal of Cu(II), Cd(II), Ni(II) and Zn(II) from aqueous solution, Appl. Surf. Sci. 314 (2014) 1063–1069.
[44] W. Yang, P. Ding, L. Zhou, J. Yu, X. Chen, F. Jiao, Preparation of diamine modified mesoporous silica on multi-walled carbon nanotubes for the adsorption of heavy metals in aqueous solution, Appl. Surf. Sci. 282 (2013) 38–45.
[45] V.N. Losev, O.V. Buyko, A.K. Trofimchuk, O.N. Zuy, Silica sequentially modified with polyhexamethylene guanidine and Arsenazo I for preconcentration and ICP–OES determination of metals in natural waters, Microchem. J. 123 (2015) 84–89.
[46] C.W. Lim, K. Song, S.H. Kim, Synthesis of PPy/silica nanocomposites with cratered surfaces and their application in heavy metal extraction, J. Ind. Eng. Chem. 18 (2012) 24–28.